RSC Advances

ROYAL SOCIETY OF CHEMISTRY

www.rsc.org/advances

Cite this: DOI: 10.1039/c0xx00000x

www.rsc.org/xxxxxx

ARTICLE TYPE

Facile Shape Design and Fabrication of $ZnFe_2O_4$ as Anode Material for Li-ion Batteries

Xiao-Bin Zhong, Bo Jin*, Zhi-Zheng Yang, Cheng Wang, Hui-Yuan Wang*

Received (in XXX, XXX) Xth XXXXXXXXX 20XX, Accepted Xth XXXXXXXXX 20XX

DOI: 10.1039/b000000x

Functional materials with exposed highly reactive planes have attracted considerable attentions with respect to their enhanced electrochemical energy storage. However, highly active facets for $ZnFe_2O_4$ nanocrystals usually have high surface energy, and thus are hard to be prepared in the equilibrium state or via the traditional methods. In this regard, we propose a novel strategy to fabricate cube, truncated octahedra, and octahedra $ZnFe_2O_4$ by a convenient hydrothermal method and subsequent thermal treatment for the first time. The $ZnFe_2O_4$ octahedron exhibits a reversible capacity of 450 mAh g^{-1} at a current density of 60 mA g^{-1} after 50 cycles, while the reversible capacity of $ZnFe_2O_4$ cube is 367 $mAhg^{-1}$. The electrochemical performance of three types of $ZnFe_2O_4$ can be ranked as "octahedra > truncated octahedra > cube". The exposed planes, which are filled with a high density of atoms, lead to the better electrochemical performance.

1. Introduction

Lithium ion batteries (LIBs) have been a great commercial success in portable electronic devices. However, the commercial LIBs do not meet the requirement for higher capacity, longer cycle life and greater safety in the electric vehicle market.[1-5] To some extent, the commercial carbon anode limits its application, because of its relatively low gravimetric capacity and poor safety. As promising candidates, transition metal oxides (such as Fe_3O_4,[6, 7] $NiFe_2O_4$,[8] $CoFe_2O_4$,[9] $ZnCo_2O_4$,[10] and $ZnFe_2O_4$[11]) have been one of the most widely investigated anode materials for LIBs over the last several years. Among them, $ZnFe_2O_4$ attracts increasing interest due to its high theoretical specific capacity (1072 mAh g^{-1}), low toxicity, and abundance, but the poor electrical conductivity limits its practical application. A vast majority of approaches have been adopted to improve the electrochemical performance of $ZnFe_2O_4$, such as carbon-based material coating,[4, 5, 12, 13] element doping[14, 15] and special structure preparing.[3, 11, 16-18]

Meanwhile, crystals with different types of exposed facets usually have great influence on the electrochemical performance. Owing to the different density of atomic steps and edges as well as abundant unsaturated coordination sites, the reactivity of high-energy facets is usually greater than that of low-energy facets.[19, 20] The high-energy facets have more metal cations in transition metal oxides. According to the previously proposed charge/discharge mechanism of transition metal oxides, the redox reaction of metal cations have great influence on their electrochemical performances.[21-25] Therefore, design and synthesis of nanostructures with exposed highly reactive crystal planes have been paid more and more attentions. For example, Li and coworkers[1] facilely synthesized cube, truncated octahedra and octahedra morphologies for Co_3O_4 by adjusting the amount of the reactants NaOH and $Co(NO_3)_2{\cdot}6H_2O$. In addition, a facile top-down approach has been reported to fabricate uniform single-crystal R-Fe_2O_3 nanodiscs through a controlled oxalic acid etching process at room temperature.[26] Single-crystal Co_3O_4 nanocages with highly exposed reactive facets were synthesized via ethylene glycol as soft templates.[27] These Co_3O_4 nanocages delivered a high reversible lithium storage capacity of 864 mAh g^{-1} at 0.2C over 50 cycles due to the high density of atomic steps in nanocages. However, highly reactive facets for $ZnFe_2O_4$ nanocrystals usually have high surface energy, and thus are hard to be prepared in the equilibrium state or via the traditional methods.

In this paper, we propose a novel strategy to fabricate three kinds of $ZnFe_2O_4$ with different exposed facets by a convenient hydrothermal method and subsequent thermal treatment. The three kinds of $ZnFe_2O_4$ with different well defined crystal plane structures are cubes with the {001} plane, truncated octahedra with {001} and {111} planes, and octahedra with the {111} plane. In this synthesis strategy, the three samples were tested at constant current densities. Among them, the octahedra with the {111} plane exhibited the most excellent cycle properties.

2. Experimental Methods

2.1 Sample Synthesis

All of the reagents used in our experiments are analytical purity and used without further purification. In a typical

fabrication, 2 mmol NH_4F and 5 mmol urea were dissolved into 35 mL deionized water by magnetic stirring at room temperature. Then 1 mmol $Zn(NO_3)_2 \cdot 6H_2O$ and 2 mmol $FeSO_4 \cdot 7H_2O$ were added into the solution. The resultant mixture was vigorously stirred for 10 min and transferred into a Teflon-lined stainless steel autoclave. The autoclave was heated at 200 ˚C. After cooling to room temperature, the precipitations were received by centrifugation, washed with water and ethanol, and dried under vacuum. Finally, the product was calcined at 450 ˚C for 4 h in air. To investigate the process of $ZnFe_2O_4$ formation, the samples were synthesized with different hydrothermal time (2 h, 12 h and 24 h).

2.2 Material characterizations

The crystalline phases were identified with X-ray diffraction (XRD, Dmax/2500PC, Rigaku, Japan) with Cu Kα radiation (λ = 1.5406 Å). X-ray photoelectron spectrum (XPS) was recorded on an ESCALAB 250 spectrometer (Perkin-Elmer) to characterize the surface composition. Field emission scanning electron microscopy (FESEM, JSM-6700F, Japan) was used to observe the morphologies.

2.3 Electrochemical measurements

Electrochemical studies were carried out at room temperature using CR2025 coin cells with lithium foil as the reference and counter electrodes. The working electrode was fabricated by coating the slurry of the active materials, conductive carbon black, and polyvinylidene fluoride (PVDF) binder in a weight ratio of 60:20:20 dispersed in N-methylpyrrolidone (NMP) onto a copper foil. Button-type test cells were assembled in an argon-filled glove box with 1 M $LiPF_6$ in ethylene carbonate, diethyl carbonate and ethylmethyl carbonate (1:1:1 vol.) as the electrolyte, fresh lithium foil as the counter electrode and Celgard 2300 as the separator. The automatic charge/discharge equipment (LAND CT2001A, Wuhan Jinno Electronics Ltd.) was used to perform the galvanostatic discharge/charge tests in a potential range of 0.01–3.0 V at 60 mA g^{-1} at room temperature, and cyclic voltammogram measurements were performed on an electrochemical workstation (CHI650D, Shanghai Chenhua Instruments Ltd.) at a scan rate of 0.1 mV s^{-1} from 0.01 to 3 V.

3. Results and Discussion

The morphologies of the products were examined by field emission scanning electron microscopy. As shown in Fig. 1, three different well-defined morphologies have been facilely controlled and synthesized, i.e cube with six {001} planes (Fig. 1a), truncated octahedron with eight {111} (Fig. 1b) and six {001} planes and octahedron with {111} planes (Fig. 1c). Interestingly, it was found that the morphology of product was strongly affected by the hydrothermal time. Namely, the cubes could be obtained when the hydrothermal time was 2 h. However, the shape changed from cube to truncated octahedra as the hydrothermal time increased to 12 h. With the reaction time further increasing to 24 h, the obtained shape transformed into an octahedral morphology. At the same time, the average size of three samples increased from 600 nm to 800 nm.

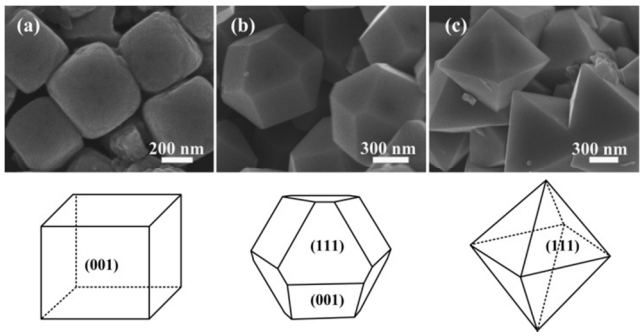

Fig.1 FESEM images of the three shapes of calcined products and their structure models: a) cubes, b) truncated octahedra and c) octahedra.

In order to identify the crystallographic structure, the calcined powder samples with different hydrothermal time were characterized by X-ray diffraction, as shown in Fig. 2. All samples exhibit a pure phase of $ZnFe_2O_4$ with a spinel structure indexed to a face-centered cubic (fcc) phase (JCPDS Card Files, No. 22-1012). No peaks from any impurities are observed in the XRD pattern. The strong intensity and narrow peak width indicate good crystallinity of the products.

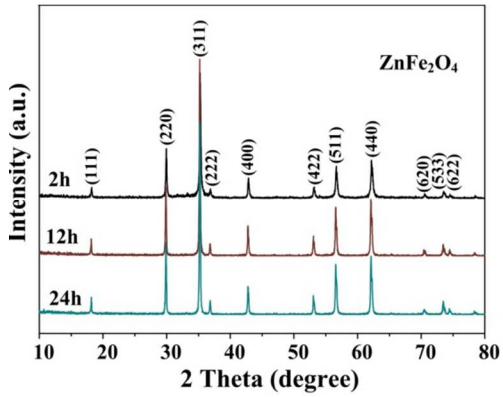

Fig.2 Comparison of XRD patterns of $ZnFe_2O_4$ for different hydrothermal time.

The composition and oxidation state of the as-prepared $ZnFe_2O_4$ were further characterized by X-ray photoelectron spectrum, as displayed in Fig. 3. The survey spectrum (Fig. 3a) could be fitted into several peaks, corresponding to C, Zn, Fe and O atoms in different forms, consistent with the formation of $ZnFe_2O_4$.[28, 29] The presence of carbon in the spectrum could be assigned to carbon contamination, because CO_2 was absorbed by the surface of the product when it was exposed to the air after synthesis.[5] The high-resolution Zn 2p XPS spectrum (Fig. 3b) shows two peaks of Zn 2p at 1020.14 and 1043.41 eV, respectively. Fig. 3c shows Fe 2p spectrum at the binding energies of 724.65 and 711.53 eV, which can be ascribed to Fe 2p1/2 and Fe 2p3/2, respectively. The binding energy of the former is 13.12 eV higher than the latter, which is consistent with that of $ZnFe_2O_4$ materials. Similar spectrum are also observed in Fig. 3d-f and Fig. 3g-i which shows the XPS measurements of the $ZnFe_2O_4$ cube and $ZnFe_2O_4$ truncated octahedra. Compared with

the intensity of Zn 2p and Fe 2p in the three examples, the differences may be caused by the different mass of examples during the measurement.

In the novel synthesis strategy, urea acted as a precipitating agent, while NH_4F played a role in structure-directing. In the hydrothermal process, urea hydrolyzed to form ammonia and alkaline environment, which is beneficial for nucleation and blocking the combination of H^+ and F^-.[30] On the other hand, free F- anions in the solution would coordinate with Zn^{2+} and Fe^{3+} on the {001} plane during the reaction, which would depress the growth along the [001] direction and promote the growth on {111} plane. According to Cornell and Schwertmann's[36] investigation, close-packed planes tend to grow more slowly and the fast-growing planes are eliminated quite rapidly. Therefore, the slow-growing planes determine the final morphology of a particle. The ratio R of the growth rates along the <001> and <111> directions determines the shape of the face-centered cubic (fcc)

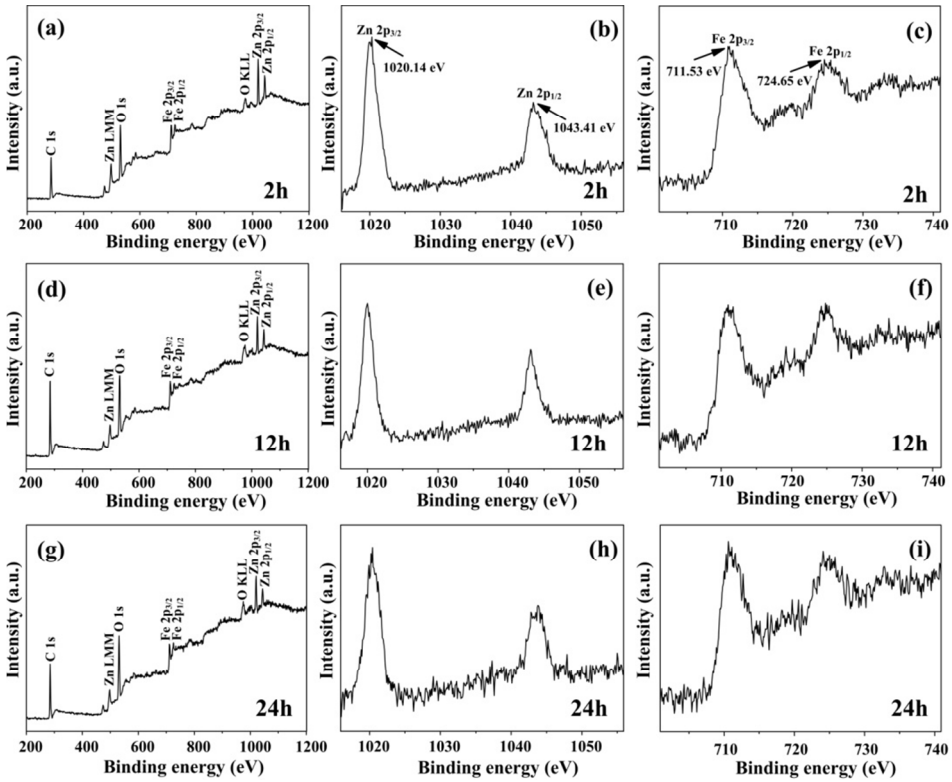

Fig. 3 XPS spectra of the $ZnFe_2O_4$ cubes, $ZnFe_2O_4$ truncated octahedra and $ZnFe_2O_4$ octahedra: (a, d, g) survey spectrum; (b, e, h) Zn2p spectrum; and (c, f, i) Fe 2p spectrum.

nanocrystal.[1, 31] When R = 0.58, 0.87, and 1.73, the cube with the {001} planes, the truncated octahedra with the {001} and {111} planes, and the octahedra with the {111} planes were formed, respectively. Based on these analyses, a possible mechanism for the formation of three different exposed facets of $ZnFe_2O_4$ was proposed. Only when the hydrothermal time was 2 h, $ZnFe_2O_4$ cubes with the exposed six {001} planes could be obtained, because {001} plane is geared to the fast-growing plane. With an increase in reaction time, alkaline condition resulting from urea hydrolyzation was conductive to the free F^-. Then the large amount of F^- would benefit the coordination of Fe^{3+} and Zn^{2+} cations on the {001} plane. The preferential adsorption of F^- anions on {001} plane depressed the growth along the [001] direction and facilitated the growth on {111} plane along with the eliminated of {001} plane. Therefore, when the hydrothermal time was increased to 12 h, the shape of $ZnFe_2O_4$ turned to be truncated octahedra. With the reaction time further increasing to 24 h, octahedral morphology was formed in the obtained $ZnFe_2O_4$. The electrochemical properties of $ZnFe_2O_4$ are examined using cyclic voltammetry (CV). Fig. 4 shows CV measurements of the $ZnFe_2O_4$ cube, $ZnFe_2O_4$ truncated octahedra and $ZnFe_2O_4$ octahedra at the first cycle. In the $ZnFe_2O_4$ octahedra, a broad peak centred at 0.70 V is observed due to the reduction of Zn^{2+} and Fe^{3+} to Zn^0 and Fe^0, the formation of Li–Zn alloys and an irreversible reaction related to the decomposition of the electrolyte.[5, 17, 32] Two typical plateaus for the $ZnFe_2O_4$ electrode at 1.56 and 1.75 V are observed in the first anodic scan process which can be ascribed to the oxidation of Zn^0 and Fe^0 to Zn^{2+} and Fe^{3+},[22, 24] respectively. Similar reduction and oxidation peaks are also observed in the $ZnFe_2O_4$ cube and $ZnFe_2O_4$ truncated octahedra electrodes. However, three obviously irreversible shallow peaks at ~1.47 V, ~0.95 V and~0.82 V can be observed in the $ZnFe_2O_4$ octahedra, which indicates the intercalation of lithium ions.[3, 15, 32] Meanwhile, only a remarkably minor shoulder is shown around 0.82 V in the $ZnFe_2O_4$ and no obviously small plateaus can be observed in the $ZnFe_2O_4$ cube. Based on these results, it can be speculated that the $ZnFe_2O_4$ octahedra is beneficial for the insertion of lithium ion.

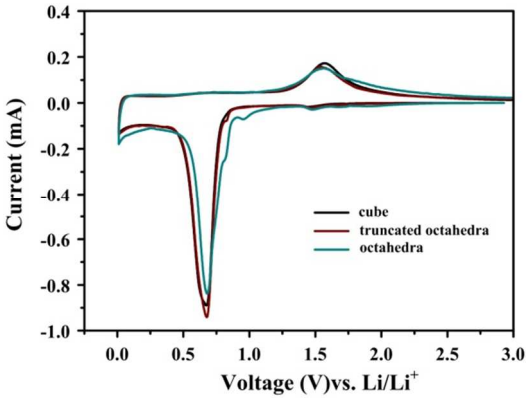

Fig. 4 Cyclic voltammograms of the $ZnFe_2O_4$ cube, $ZnFe_2O_4$ truncated octahedra, and $ZnFe_2O_4$ octahedra electrode at the first cycle between 0.01 and 3 V vs. Li^+/Li, recorded at a potential scanning rate of 0.1 mVs^{-1}.

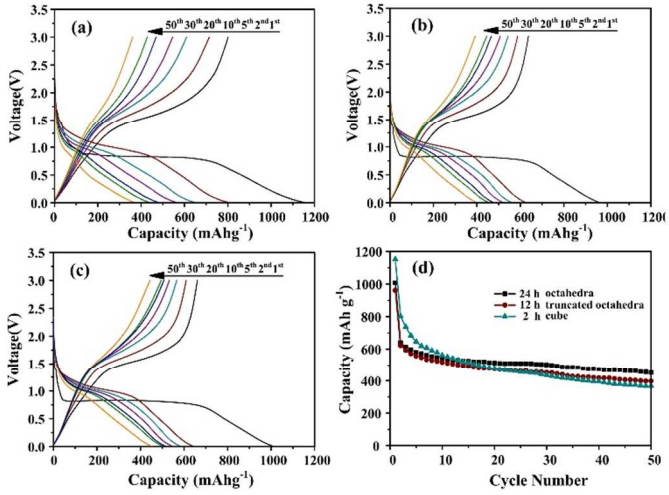

Fig. 5 The charge/discharge curves of a) $ZnFe_2O_4$ cubes, b) $ZnFe_2O_4$ truncated octahedra, and c) $ZnFe_2O_4$ octahedra for the 1st, 2nd, 5th, 10th, 20th, 30th, and 50th cycles between 0.01 and 3.0 V at a rate of 60 mA g^{-1}. d) Comparison of cycling performance of the three kinds of $ZnFe_2O_4$.

Fig. 5 shows the charge/discharge curves of the three shapes of $ZnFe_2O_4$, which were obtained at a current density of 60 mA g^{-1} in the potential window of 0.01 to 3.0 V (versus Li/Li^+). As shown in Fig. 5, all of the discharge and charge curves show voltage plateaus at about 0.7 and 1.7 V, respectively, corresponding to redox reactions during lithium insertion/extraction. After the first cycle, the discharge plateau change into a slope during the discharge/charge process. The change of the voltage plateau and the significant capacity loss after the first cycle are consistent with the shifting and damping of the peaks in the CV profiles. As depicted, the initial discharge and charge specific capacities reach about 1151 and 801 mAh g^{-1} for $ZnFe_2O_4$ cubes, 960 and 637 mAh g^{-1} for $ZnFe_2O_4$ truncated octahedra, and 1006 and 661 mAh g^{-1} for $ZnFe_2O_4$ octahedra,, respectively. The extra capacity over the theoretical specific capacity may arise from the formation of a solid electrolyte interphase (SEI) layer, the insertion of lithium ions into acetylene black and interfacial storage.[1, 22] It should be noted that the initial specific capacities show a trend of decline from $ZnFe_2O_4$ cubes to $ZnFe_2O_4$ octahedra, which can be attributed to the increase of the particle size of $ZnFe_2O_4$ and the formation of a solid electrolyte interphase (SEI) layer and possibly interfacial lithium storage.[8, 21] Firstly, the small particle size can effectively shorten the reaction pathway of Li ions, increase the electron/ion conductance and then lead to a higher capacity.[33] Moreover, the $ZnFe_2O_4$ cubes have the higher surface area exposure to electrolyte, which might also cause the higher initially discharge capacity. Therefore, the $ZnFe_2O_4$ cubes possess the highest initial capacity. Fig. 5d displays the cycle properties of $ZnFe_2O_4$ cubes, truncated octahedra, and octahedra. The discharge capacities for $ZnFe_2O_4$ cubes, truncated octahedra, and octahedra after 50 cycles are 367, 397, and 450 mAh g^{-1}, respectively. The retention rates of the discharge capacity are 45.8% (801 mAh g^{-1} after 2 cycles and 367 mAh g^{-1} after 50 cycles), 63.8% (622 mAh g^{-1} after 2 cycles and 397 mAh g^{-1} after 50 cycles) and 70.42% (639 mAh g^{-1} after 2 cycles and 450 mAh g^{-1} after 50 cycles), respectively. Even through all of the three kinds of $ZnFe_2O_4$ possess relatively excellent cycling ability, the $ZnFe_2O_4$ octahedra exhibit the highest discharge capacity and the lowest loss of discharge capacity, and $ZnFe_2O_4$ truncated octahedra ranks the second place.

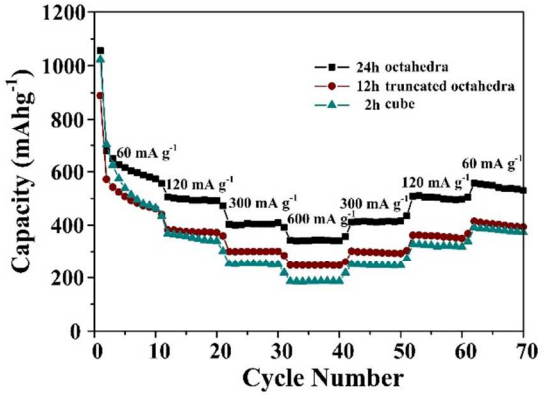

Fig. 6 Rate capability performance of the samples at different rates (increased from 60 mA g^{-1} to 600 mA g^{-1}).

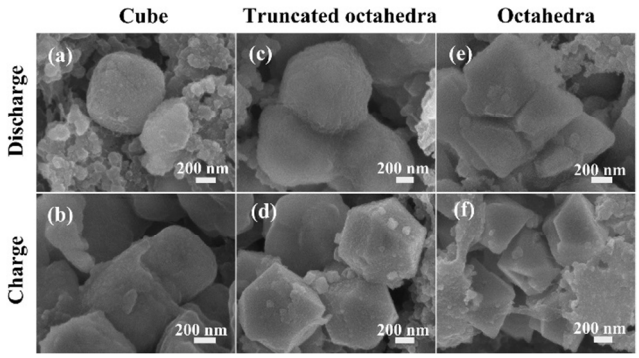

Fig. 7 The SEM images of the three composite electrodes on Cu foil after 6 discharge/charge cycles. (a, b) $ZnFe_2O_4$ cube, (c, d) $ZnFe_2O_4$ truncated octahedra and (e, f) $ZnFe_2O_4$ octahedra.

To better understand the advantage of the $ZnFe_2O_4$ octahedral structures in lithium storage, the rate capability of the three examples were investigated (Fig 6). Obviously, the specific capacity of the $ZnFe_2O_4$ octahedra was far better than that of the $ZnFe_2O_4$ truncated octahedra and cubes at all investigated discharge rates from 60 to 600 mA g^{-1}. For example, the $ZnFe_2O_4$ octahedra exhibited much superior rate performance with 472 and 408 mAh g^{-1}, which was much larger than that of the $ZnFe_2O_4$

truncated octahedra (371 and 301 mAh g^{-1}) and cubes (339 and 250 mAh g^{-1}), at current densities of 120 and 300 mA g^{-1}, respectively. At the high current rate of 600 mA g^{-1}, the capacities of $ZnFe_2O_4$ truncated octahedra and cubes decreased to only about 245 mAh g^{-1} and 185 mAh g^{-1}, respectively, but the capacity of $ZnFe_2O_4$ octahedra was still up to about 341 mAh g^{-1}. In order to further recognize the effects of exposed planes on the electrochemical properties of $ZnFe_2O_4$, we examined their morphology change after electrochemical cycles (Fig 7). It is obviously demonstrated that the morphology of the examples can be retained. Compared the morphology after discharge and charge, the surface of the discharge turned into more rough with the insertion of Li^+. Even though the pulverization of the particles could not be eliminated during cycling that leads to the poor cycling stability, the pulverization could be delayed by the initially exposed high-energy facets.[34, 35]

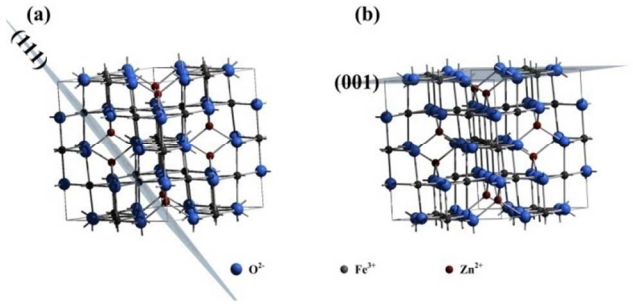

Fig. 8 The surface atomic configurations in the (001) plane and (111) plane of $ZnFe_2O_4$.

The three types of $ZnFe_2O_4$ present different electrochemical performances due to the crystal plane effect and the crystal plane structure. Li and coworkers[1] have confirmed that the {111} plane has more Co^{2+} than the {001} plane in Co_3O_4, which is similar to the case of Zn^{2+} in the $ZnFe_2O_4$, as shown in Fig. 8. As illustrated in Figure 8a, 3 Fe^{3+} and 1 Zn^{2+} belong to (111) facets, while only 2 Fe^{3+} and 1 Zn^{2+} are present in (001) facets in Figure 8b. The {111} plane is beneficial for the coordination of Fe^{3+} with Li^+. The $ZnFe_2O_4$ octahedra has a greater area of exposed {111} planes and faster Fe^{3+}/Fe redox reaction, which brings about the highest capacity.

4. Conclusions

In summary, we have facilely designed and fabricated cube, truncated octahedra, and octahedron $ZnFe_2O_4$ by a convenient hydrothermal method and subsequent thermal treatment for the first time. In the process of hydrothermal reaction, urea acted as a precipitating agent, while NH_4F played a role in structure-directing. It was found that the morphology of $ZnFe_2O_4$ was strongly affected by the hydrothermal time. With the increasing of hydrothermal time, the shape of $ZnFe_2O_4$ changes from cube to octahedra. According to the comparison of the three types of $ZnFe_2O_4$, their electrochemical performance can be ranked as "octahedra > truncated octahedra > cube". The results show that the crystal plane structure of electrode materials has great influence on the electrochemical performance of $ZnFe_2O_4$.

Acknowledgements

The authors acknowledge financial support from Foundation of Jilin University for Distinguished Young Scholars and Project 985-Materials Science and Engineering of Jilin University.

Notes and references

Key Laboratory of Automobile Materials, Ministry of Education, and College of Materials Science and Engineering, Jilin University, Changchun 130025, China.
E-mail: wanghuiyuan@jlu.edu.cn; Tel.: +86 0431 85094699.
E-mail: jinbo@jlu.edu.cn; Tel.:+86 0431 85095170

1. X. Xiao, X. Liu, H. Zhao, D. Chen, F. Liu, J. Xiang, Z. Hu and Y. Li, *Advanced materials*, 2012, **24**, 5762.
2. B. Lim, J. Jin, J. Yoo, S. Y. Han, K. Kim, S. Kang, N. Park, S. M. Lee, H. J. Kim and S. U. Son, *Chemical communications*, 2014, **50**, 7723.
3. P. F. Teh, Y. Sharma, S. S. Pramana and M. Srinivasan, *Journal of Materials Chemistry*, 2011, **21**, 14999.
4. J. Sui, C. Zhang, D. Hong, J. Li, Q. Cheng, Z. Li and W. Cai, *Journal of Materials Chemistry*, 2012, **22**, 13674.
5. Y. K. Jong Guk Kim, Yuseong Noh and Won Bae Kim, *RSC Advances*, 2014.
6. L. Shen, H. Song, H. Cui, X. Wen, X. Wei and C. Wang, *CrystEngComm*, 2013, **15**, 9849.
7. B. Jin, A.-H. Liu, G.-Y. Liu, Z.-Z. Yang, X.-B. Zhong, X.-Z. Ma, M. Yang and H.-Y. Wang, *Electrochimica Acta*, 2013, **90**, 426.
8. G. Huang, F. Zhang, L. Zhang, X. Du, J. Wang and L. Wang, *Journal of Materials Chemistry A*, 2014, **2**, 8048.
9. A. K. Rai, J. Gim, T. V. Thi, D. Ahn, S. J. Cho and J. Kim, *The Journal of Physical Chemistry C*, 2014, **118**, 11234.
10. J. Bai, X. Li, G. Liu, Y. Qian and S. Xiong, *Advanced Functional Materials*, 2014, **24**, 3012.
11. L. Yao, X. Hou, S. Hu, Q. Ru, X. Tang, L. Zhao and D. Sun, *Journal of Solid State Electrochemistry*, 2013, **17**, 2055.
12. H. Xia, Y. Qian, Y. Fu and X. Wang, *Solid State Sciences*, 2013, **17**, 67.
13. J. Xie, W. Song, G. Cao, T. Zhu, X. Zhao and S. Zhang, *RSC Advances*, 2014, **4**, 7703.
14. A. S. Hameed, H. Bahiraei, M. V. Reddy, M. Z. Shoushtari, J. J. Vittal, C. K. Ong and B. V. Chowdari, *ACS applied materials & interfaces*, 2014, **6**, 10744.
15. D. Bresser, F. Mueller, M. Fiedler, S. Krueger, R. Kloepsch, D. Baither, M. Winter, E. Paillard and S. Passerini, *Chemistry of Materials*, 2013, **25**, 4977.
16. X. Guo, X. Lu, X. Fang, Y. Mao, Z. Wang, L. Chen, X. Xu, H. Yang and Y. Liu, *Electrochemistry Communications*, 2010, **12**, 847.
17. Y. Deng, Q. Zhang, S. Tang, L. Zhang, S. Deng, Z. Shi and G. Chen, *Chemical communications*, 2011, **47**, 6828.
18. X. Guo, H. Zhu, M. Si, C. Jiang, D. Xue and Q. Li, *CrystEngComm*, 2013, **15**, 8306.
19. N. Tian, Z. Y. Zhou, S. G. Sun, Y. Ding and Z. L. Wang, *Science*, 2007, **316**, 732.
20. Z.-Y. Z. Na Tian, Neng-Fei Yu, Li-Yang Wang, and Shi-Gang Sun, *J. AM. CHEM. SOC*, 2010, **132**, 7580.
21. L. Li, H. B. Wu, L. Yu, S. Madhavi and X. W. D. Lou, *Advanced Materials Interfaces*, 2014, n/a.
22. Z. Xing, Z. C. Ju, J. Yang, H. Y. Xu and Y. T. Qian, *Nano Research*, 2012, **5**, 477.
23. J. Luo, J. Liu, Z. Zeng, C. F. Ng, L. Ma, H. Zhang, J. Lin, Z. Shen and H. J. Fan, *Nano letters*, 2013, **13**, 6136.
24. D. L. G. Binotto, A. S. Prakash,R. Herrera Urbina,M.S. Hegde,and J-M. Tarascon, *Chem. Mater*, 2007, **19**, 3032.
25. S. W. Chunnian He, Naiqin Zhao, Chunsheng Shi, Enzuo Liu, and Jiajun Li, *ACS nano*, 2013, **7**, 4459.

26. T. Z. Jun Song Chen, Xiao Hua Yang,Hua Gui Yang,and Xiong Wen Lou, *J. AM. CHEM. SOC*, 2010, **132**.
27. D. Liu, X. Wang, X. Wang, W. Tian, Y. Bando and D. Golberg, *Scientific reports*, 2013, **3**, 2543.
28. D. Zhao, Y. Xiao, X. Wang, Q. Gao and M. Cao, *Nano Energy*, 2014, **7**, 124.
29. Y. H. Hai-Sheng Qian, Zheng-Quan Li,Xing-Yun Yang,Liang-Chao Li,Xian-Ting Zhang,and Rong Xu, *J. Phys. Chem. C*, 2010, **114**, 17455.
30. B. Lv, Z. Liu, H. Tian, Y. Xu, D. Wu and Y. Sun, *Advanced Functional Materials*, 2010, **20**, 3987.
31. Z. L. Wang, *J. Phys. Chem. B*, 2000, **104**, 1153.
32. F. Martinez-Julian, A. Guerrero, M. Haro, J. Bisquert, D. Bresser, E. Paillard, S. Passerini and G. Garcia-Belmonte, *The Journal of Physical Chemistry C*, 2014, **118**, 6069.
33. X. Yu, H. Pan, W. Wan, C. Ma, J. Bai, Q. Meng, S. N. Ehrlich, Y. S. Hu and X. Q. Yang, *Nano letters*, 2013, **13**, 4721.
34. M. Zhang, D. Lei, X. Yin, L. Chen, Q. Li, Y. Wang and T. Wang, *Journal of Materials Chemistry*, 2010, **20**, 5538.
35. G. Zhou, D.-W. Wang, F. Li, L. Zhang, N. Li, Z.-S. Wu, L. Wen, G. Q. Lu and H.-M. Cheng, *Chemistry of Materials*, 2010, **22**, 5306.
36. R. M. Cornell, U. Schwertmann, The Iron Oxides: Structure, Properties, Reactions, Occurrences and Uses Wiley-VCH Weinheim 2003.